SYNTHESIS OF NANOPARTICLES VIA SURFACE MODIFICATION FOR ELECTRONIC APPLICATIONS

Burtrand I. Lee and Song Wei Lu[a]
Department of Ceramic and Materials Engineering, Olin Hall, P. O. Box 340907, Clemson University, Clemson, SC 29634-0907, USA

[a]Currently at Oak Ridge National Laboratory, Oak Ridge, TN 37830

ABSTRACT

The demand for sub-micrometer or nanometer functional ceramic powders with a better suspension behavior in aqueous media is increasing. Redispersible barium titanate (BT) nanocrystals, green light emitting Mn^{2+} doped Zn_2SiO_4 and ZnS nanoparticle phosphors were synthesized by a hydrothermal method or chemical precipitation with surface modification. The nanoparticle redispersibility for BT was achieved by using a polymeric surfactant. X-ray diffraction (XRD) results indicated that the BT particles are of cubic phase with 80 nm in size.

XRD results of zinc silicate phosphor indicate that seeds play an important role in enhancing the nucleation and crystallization of Zn_2SiO_4 crystals in a hydrothermal condition. This paper describes and discuss the methods of surface modification, and the resulting related properties for BT, zinc silicate and zinc sulfide.

KEYWORDS: Barium titanate; Nanoparticles; Luminescence; Mn^{2+} doped ZnS; Surface passivation; Seeding; Zinc silicate.

INTRODUCTION

The usefulness of nanosized ceramic functional particles are increasingly recognized. Due the high surface area to volume ratio of these particles, processing difficulty of handling and processing are often encountered. The demand for nano-size dielectric ceramic particles has increased due to the development of volume-efficient multilayer ceramic capacitors (MLCCs).

prevent nanoparticle agglomeration in the solution [26]. PL enhancement up to ten-fold has been observed for polymethyl merthacrylate (PMMA) coated ZnS nanocrystals doped with Mn^{2+} ions [27,28].

This paper describes chemical techniques to modify the surface for enhanced properties and processability for nanosized particles. The PL enhancement mechanism for Mn^{2+} doped ZnS nanoparticles modified with a surface modifying agent has not been adequately addressed in the literature, especially the role of a PAL on PL enhancement.

EXPERIMENTAL

Nano BT was synthesized by using an aqueous solution of $BaCl_2$ mixed with an aqueous solution of $TiCl_4$. Polyoxyethylene (20) sorbitan monooleate (Tween®80) was added as a polymeric stabilizer into above solution at a concentration of 5.0 wt%. A high pH was maintained by KOH. The resulting milky sol filled a high-pressure stainless steel vessel. The sealed vessel was heated to 100 °C ~ 230 °C for 10 min to 2 h. The resultant nanocrystals were washed with deionized water and dried .

For zinc silicate tetraethyl orthosilicate (TEOS) sol, which had been hydrolyzed by a water/TEOS molar ratio of 2, was added to a stoichiometric solution of $Mn(CH_3COO)_2{\cdot}4H_2O$ and $Zn(CH_3COO)_2{\cdot}2H_2O$ in ethanol and deionized water at room temperature for Mn^{2+} doping concentration of 2 mole%. Tween80 was added as a surface modifier to the above solution and the sol was adjusted to pH = 10 by ammonium hydroxide. The zinc silicate sol filled a stainless steel vessel along with Zn_2SiO_4:Mn^{2+} seed particles (5wt% with respect to the final products). The seed particles were obtained by firing a 25 ml volume of the above sol at 1000°C for 2 h in air. The sealed vessel was then heated to 230°C for 2 h. After cooling down to room temperature, the resultant precipitate was centrifuged and washed with deionized water several times followed by drying at 60°C for 24 h in a vacuum oven.

Mn^{2+} doped ZnS nanocrystals were synthesized by a chemical precipitation method at room temperature using $Zn(CH_3COO)_2{\cdot}2H_2O$, $Mn(CH_3COO)_2{\cdot}4H_2O$, and $Na_2S{\cdot}9H_2O$ as starting

prevent nanoparticle agglomeration in the solution [26]. PL enhancement up to ten-fold has been observed for polymethyl merthacrylate (PMMA) coated ZnS nanocrystals doped with Mn^{2+} ions [27,28].

This paper describes chemical techniques to modify the surface for enhanced properties and processability for nanosized particles. The PL enhancement mechanism for Mn^{2+} doped ZnS nanoparticles modified with a surface modifying agent has not been adequately addressed in the literature, especially the role of a PAL on PL enhancement.

EXPERIMENTAL

Nano BT was synthesized by using an aqueous solution of $BaCl_2$ mixed with an aqueous solution of $TiCl_4$. Polyoxyethylene (20) sorbitan monooleate (Tween®80) was added as a polymeric stabilizer into above solution at a concentration of 5.0 wt%. A high pH was maintained by KOH. The resulting milky sol filled a high-pressure stainless steel vessel. The sealed vessel was heated to 100 °C ~ 230 °C for 10 min to 2 h. The resultant nanocrystals were washed with deionized water and dried .

For zinc silicate tetraethyl orthosilicate (TEOS) sol, which had been hydrolyzed by a water/TEOS molar ratio of 2, was added to a stoichiometric solution of $Mn(CH_3COO)_2{\cdot}4H_2O$ and $Zn(CH_3COO)_2{\cdot}2H_2O$ in ethanol and deionized water at room temperature for Mn^{2+} doping concentration of 2 mole%. Tween80 was added as a surface modifier to the above solution and the sol was adjusted to pH = 10 by ammonium hydroxide. The zinc silicate sol filled a stainless steel vessel along with Zn_2SiO_4:Mn^{2+} seed particles (5wt% with respect to the final products). The seed particles were obtained by firing a 25 ml volume of the above sol at 1000°C for 2 h in air. The sealed vessel was then heated to 230°C for 2 h. After cooling down to room temperature, the resultant precipitate was centrifuged and washed with deionized water several times followed by drying at 60°C for 24 h in a vacuum oven.

Mn^{2+} doped ZnS nanocrystals were synthesized by a chemical precipitation method at room temperature using $Zn(CH_3COO)_2{\cdot}2H_2O$, $Mn(CH_3COO)_2{\cdot}4H_2O$, and $Na_2S{\cdot}9H_2O$ as starting

materials. A 50 ml ethanol solution was prepared by dissolving 2.195 g $Zn(CH_3COO)_2 \cdot 2H_2O$ and 0.049 g $Mn(CH_3COO)_2 \cdot 4H_2O$ with stirring at room temperature. This yielded a Mn^{2+} doping concentration of 2 mole%. Then, a 50 ml aqueous solution of 2.451 g $Na_2S \cdot 9H_2O$ was added to the ethanol solution drop by drop with vigorous stirring. The resultant white precipitate was centrifuged and washed using deionized water. Finally, 1.987 g of 3-methacryloxypropyl trimethoxysilane (MPTS) was added to the resultant mixture after centrifuging and washing. In order to compare the effect of a passivating additive on luminescence properties, 0.5 g Tween® 80 was added to the resultant precipitate in the second sample. The third sample was prepared without the addition of the surface modifying agent.

Transmission electron microscopy (TEM) study of these nanocrystals was carried out at 200 kV using a Hitachi HF-2000 TEM equipped with a field emission source. The TEM specimens were prepared by dispersing the as-prepared Mn^{2+} doped ZnS nanoparticles in methane, and picking up the nanocrystals using a carbon film supported by a copper grid. The UV-visible absorption spectrum was obtained in a Hitachi 5000 spectrophotometer for Mn^{2+} doped ZnS nanoparticles coated on a silica glass substrate. This sample was prepared by dip-coating from a colloidal solution of ZnS and drying at room temperature in air.

The particle size and size distribution were characterized using a Horiba LA-910 laser scattering particle size analyzer. The samples were dispersed in distilled water and ultrasonically treated for 10 min prior to the size analysis. X-ray diffraction (XRD) measurements were performed using an XDS X-ray diffractometer (Model 2000, Scintag, Inc.) from $2\theta = 20°$ to 80 ° with a scan step of 0.02 °. Thermogravimetric analysis (TGA) measurement was performed by a NETZSCH STA 449C TGA unit in argon atmosphere from 50 °C to 1300 °C with a heating rate of 10 $°C \cdot min^{-1}$.

For PL measurements, above bandgap excitation was achieved by using the 275 nm (4.51eV) line from an argon ion laser. The laser power was reduced to an appropriate level by using a set of neutral density filters to avoid local heating. Typical excitation intensities were between 300$mW \cdot cm^{-2}$ and 1$W \cdot cm^{-2}$. The PL signal was dispersed by a 1000M Spex monochromator and

detected by a thermoelectrically cooled GaAs photomultiplier tube (PMT) operating in the photon counting mode.

RESULTS AND DISCUSSION

Figure 1 shows a TEM bright field image of BT nanocrystals synthesized with a pH of 13.5 at 230 °C for 0.5 h. It can be seen that BT particles are well-dispersed and in spherical forms. Some particles are weakly agglomerated due to the large amount of particles presented in the TEM image. The EDS results confirmed that the chemical composition of particles is $BaTiO_3$.

The mean particle diameter was statistically estimated to be 77.4±27.6 nm from approximately 250 particles in the TEM image, as shown in Fig. 1. In order to compare the results, the mean particle size was also measured by a Horiba particle size analyzer based on a laser scattering method. The size distribution from laser scattering method was 83 ±19 nm. It is noted that the mean particle size measured from laser scattering method is larger than the estimation from the TEM image. This is due to the fact that polymeric species, anchored on particle surface, have been taken into account during the laser scattering method, i. e., the polymer coated particles are slightly larger than the BT particles themselves.

In order to determine the phase of BT particles, XRD analyses were performed. Fig. 2 presents the XRD patterns of BT nanoparticles synthesized at 150 °C for 30 min from the precursor with different pH values. From a solution with a pH of 12.0, there is no crystallization after hydrothermal treatment. When the precursor pH was raised to 12.8, BT nanocrystals became detectable. However, there is an unexpected peak at $2\theta = 24$ ° (marked with *), whose origin is unclear. It might belong to an intermediate phase or carbonate. For the precursor sol with a pH of 13.5, all peaks from the XRD pattern match well with standard cubic BT phase JCPDS No. 31-174.

Fig. 3 shows the DSC results of BT nanoparticles synthesized from a precursor of pH = 13.5

at 230 °C for 0.5 h. It has been shown in DSC results that there is no endo-thermal peak between 50 °C and 150 °C, indicative of no phase transition around the BT Curie point between 125 °C and 130 °C. It is, therefore, suggested that the BT particles synthesized by the hydrothermal method have a cubic structure. There are three exo-thermal peaks at 171 °C, 344 °C, and 426 °C, which correspond to the burnout of organic species from BT nanoparticle surfaces.

Although the phase of BT nanoparticles have been confirmed as cubic phase from both XRD and DSC results, a debate on actual phase of BT nanoparticles remains in the literature. This debate originated from the detection of Raman-active modes attributing to tetragonal BT (*p4mm*) by using Raman spectroscopy from BT nanoparticles whose XRD patterns showing a cubic phase (*pm3m*). During nucleation and crystallization of BT nanocrystals, Tween® 80 acted as a surface modifier and growth inhibitor for the particles. Tween® 80 has a hydrophilic head group and a hydrophobic tail as shown in Fig. 4. The presence of these polymeric species prevents the agglomeration of particles and hinders the further growth of individual particles. Tween® 80 can also be used as a steric stabilizer while dispersing resultant BT nanoparticles in aqueous media. The polymeric species on BT particle surface act as a dispersant in water, leading to a better redispersibility of the synthesized nanoparticles. The better redispersibility of BT nanocrystals is actually due to the steric stabilization of the particles in the presence of Tween® 80 on the particle surface.

Fig. 5 shows the X-ray diffraction (XRD) pattern of the Mn^{2+} doped Zn_2SiO_4 phosphor particles synthesized by the seeded hydrothermal method. In order to compare the seeding effect on crystallization, the XRD pattern of samples without seeds after the same hydrothermal reaction was also measured. The XRD pattern of the Mn^{2+} doped Zn_2SiO_4 seeds after firing at 1000 °C for 2 h in air is also presented for comparison. It is shown in Fig.5 that the XRD patterns of both Zn_2SiO_4:Mn^{2+} seeds and phosphor samples after a seeded hydrothermal reaction agree very well with those in the literature for Zn_2SiO_4 crystals [29]. However, no Zn_2SiO_4 crystallization, under the same condition, was detected from a sample without seeds, whose XRD pattern shows only weak intermediate peak at $2\theta = 45$. In the present work,

Zn_2SiO_4 crystals were well developed after only 2 h at 230°C in a seeded hydrothermal method. Thus, seeding brings a positive effect on heterogeneous nucleation sites lowering the supersaturation necessary for crystallization.

Fig. 6 displays a transmission electron microscopy (TEM) image of the Mn^{2+} doped Zn_2SiO_4 phosphor particles. The particles are non-spherical with a mean length of 700 nm and a mean width of 350 nm. These particles are uniform without agglomeration. The PL spectrum of our Mn^{2+} doped Zn_2SiO_4 phosphor particles is shown as curve 1 in Fig. 7 (a) with the emission maximum located at 522 nm, attributable to the ^4G-^6S transition in Mn^{2+} doping centers. The seeding effect is apparent that no green photoluminescence was observed from particles without seeds. This is in good agreement with the XRD results that no Zn_2SiO_4 crystallization was detected from the sample without seeds.

HRTEM images in Fig. 8 show well-defined nanocrystals whose size was estimated to be about 2.8 nm. The lattice fringe is clearly exhibited from an individual nanocrystal, whose lattice constant d was evaluated as 3.11 Å. This is in good agreement with lattice constant of cubic ZnS with a d of 3.123 Å for {111} plane. The peak broadening in the XRD pattern clearly indicates that very small nanocrystals are present in the samples. From the width of the XRD peak (Fig. 9) broadening, the mean crystalline size can be calculated using Scherrer's equation: $D = 57.3\ k\lambda/\beta\cos\theta$, where k is a geometric factor taken to be 1, λ is the X-ray wavelength (for Cu Ka radiation, $\lambda = 1.541$ Å), θ is the diffraction angle, and β is the half-width of the diffraction peak at 2θ. The mean crystal size of Mn^{2+} doped ZnS nanoparticles is calculated to be 2.6 nm with a calculation error of 15 %, i.e. 2.6 ± 0.4 nm. This is consistent with the estimated size from nanocrystals in HRTEM images. No apparent difference was observed in the XRD peak shape and broadening of Mn^{2+} doped ZnS nanoparticles before and after surface passivation.

PL properties of Mn^{2+} doped ZnS nanoparticles were characterized for samples with MPTS, with Tween® 80, and without additives as shown in Fig. 9. An orange photoluminescence was observed from Mn^{2+} doped ZnS nanocrystals without MPTS whose peak is located at 601 nm. It is also shown in Fig. 9 that the PL intensity of Mn^{2+} doped ZnS nanocrystals

passivated by MPTS was enhanced by a 30-fold, in comparison with the samples without MPTS passivation. No orange photoluminescence from MPTS alone was observed after UV excitation at 275 nm. This confirms that the enhanced PL is not from MPTS itself but from surface passivated nanoparticles. In contrast, the PL intensity of Mn^{2+} doped ZnS nanoparticles coated with Tween® 80 remained the same as that without the surface agent. This indicates that not all surface absorbates effective enhancing photoluminescence of Mn^{2+} doped ZnS nanoparticles by surface passivation. Gallagher et al. [30] also did not observe any photoluminescence enhancement in Mn^{2+} doped ZnS nanocrystals coated with poly ethylene oxide.

The PL enhancement can be explained by a passivation of the surface defects on nanoparticles. Since non-radiative recombination occurs through these surface defects, the radiative probability through the Mn^{2+} centers decreases with increasing surface defects. It is, therefore, expected that an enhancement of the radiative probability will be achieved by an elimination of the surface defects through surface passivation. In the presence of MPTS as a surface modifier, the surface defects on Mn^{2+} doped ZnS nanoparticles are passivated and eliminated. Hence, an increase of the radiative transition through Mn^{2+} centers is accomplished.

PL enhancement by MA or PMMA has been reported [26-28]. A common functional group in MPTS and PMMA is a caboxylic/ester groups as shown in Fig 10. Comparing MPTS with MA and PMMA, it is believed that the carboxylic/ester groups from these PALs play a significant role in enhancing the PL intensity. Isobe et al. [26] verified the chemical interaction between sulfur on ZnS:Mn^{2+} nanoparticles surface and oxygen of carboxylic acid in MA by X-ray photoelectron spectroscopy (XPS). They concluded that the carboxylic group anchors on particle surface after formation of Mn^{2+} doped ZnS nanoparticles. Surface passivation of the defects by the presence of a passivating coating is, therefore, achieved. However, not all surface passivating agents containing carboxylic functional groups showed PL enhancement effect for Mn^{2+} doped ZnS nanoparticles. Tween® 80, a polyethylene of sorbitan oleate, played no role in PL enhancement. It is well-known that the carboxylic-ester groups can have resonance structure and inductive effect by the chemical nature of the molecular structure. The resonance/inductive

effect can be ineffective if there is a severe steric hindrance. Tween® 80 does have the steric hindrance from long chains both sides of the carboxylic-ester group. It is believed that this steric hindrance hinders the adsorption of Tween® 80 molecules on the nanoparticle surface via the carboxylic-ester group. Hence, Tween® 80 must adsorbe on nanoparticle surface via -OH groups. In comparing MPTS with Tween® 80, the resonance/inductive effect makes interaction of the carboxylic-ester group on nanoparticle enhanced, leading to a surface passivation of the nanoparticles in the presence of the functional group. On the other hand, polyethylene oxide, which has no carboxylic groups in its long chain, has no luminescence enhancement effect for Mn^{2+} doped ZnS nanoparticles [30].

CONCLUSIONS

Redispersible BT nanocrystals have been synthesized by using a hydrothermal method at low temperature in the presence of a surface modifier. The particle size of BT nanoparticles synthesized at 230 °C for 0.5 h is estimated to be 77.4 ±27.6 nm from TEM image, and 83 _ 19 nm from a laser scattering particle size analyzer. XRD and DSC results suggest that the particles are in cubic phase. BT nanoparticles can be formed at temperatures as low as 100 °C, in reaction time more than 10 min, and precursor pH of 13.5. The redispersibility of BT nanoparticles is excellent, resulting from a steric stabilization of particles in the presence of Tween® 80 on the nanoparticle surface.

Green light emitting Mn^{2+} doped Zn_2SiO_4 particles were produced using a seeded hydrothermal method. The addition of seeds enhanced the nucleation and crystallization of Zn_2SiO_4 crystals. This was translated into enhanced PL of the seeded hydrothermal phosphor as compared with the corresponding unseeded phosphors. Both photoluminescence and cathodoluminescence were observed from these Mn^{2+} doped Zn_2SiO_4 phosphor particles.

An enhanced photoluminescence of Mn^{2+} doped ZnS nanoparticles have been demonstrated by chemical precipitation at room temperature in the presence of MPTS as a PAL. A 30-fold

enhancement has been observed after the surface passivation. This is achieved by eliminating the surface defects, in which the carboxylic groups with effective resonance/inductive effect in the surface modifying agent plays an important role.

Acknowledgement

We wish to thank the U.S. National Science Foundation and American Chemical Society's Petroleum Research Fund Type AC for the financial support for this research. Various technical support from the Phosphor Technology Center of Excellence at Georgia Institute of Technology is gratefully acknowledged.

REFERENCES

1. L. K. Templeton, and J. A. Pask, J. Am. Ceram. Soc., **42** [5] (1959) 212-216.
2. A. Beauger, J. C. Mutin, and J. C. Niepce, J. Mater. Sci., **18**, (1983) 3543-3550.
3. M. Wu, R. Xu, S. H. Feng, L. Li, D. Chen, and Y. J. Luo, J. Mater. Sci., **31**, (1996) 6201-6205.
4. C. T. Xia, E. W. Shi, W. E. Zhong, J. K. Guo, J. Euro. Ceram. Soc., **15** [12] (1995) 1171-1176.
5. E. B. Slamovich and I. A. Aksay, J. Am. Ceram. Soc., **79** [1] (1996) 239-247.
6. L. Zhao, A. T. Chien, F. F. Lapse, and J. S. Speck, J. Mater. Res., **11** [6] (1996) 1325-1328.
7. R. Viekanandan, and T. R. N. Kutty, Powder Tech., **57**, (1998) 181-192.
8. G. Busa, V. Buscaglia, M. Leoni, and P. Nanni, Chem. Mater., **6**, (1994) 955-961.
9. T. Noma, S. Wada, M. Yano, and T. Suzuki, J. Appl. Phys., **80** [9] (1996) 5223-5233.
10. R. Asiaie, W. Zhu, S. A. Akbar, and P. K. Dutta, Chem. Mater., **8**, (1996) 226-234.
11. I. J. Clark, T. Takeuchi, N. Ohtori, and D. C. Sinclair, J. Mater. Chem., **9**, (1999) 83-91.
12. D. Hennings, and S. Schreinmacher, J. Euro. Ceram. Soc., **9**, (1992) 41-46.
13. E. W. Shi, C. T. Xia, W. E. Zhong, B. G. Wang, and C. D. Feng, J. Am. Ceram. Soc., **80** [6] (1997) 1567-1572.
14. J. O. Eckert, Jr., C. C. Hung-Houston. B. L. Gersten, M. M. Lencka, and R. E. Riman, J. Am. Ceram. Soc., **79** [11] (1996) 2929-2939.
15. P. K. Dutta, R. Asiaie, S. A. Akbar, and W. D. Zhu, Chem. Mater., **6**, (1994) 1542-1548.
16. P. K. Dutta, and J. R. Gregg, Chem. Mater., **4** [4] (1992) 843-846.
17. A. J. I. Ward, and S. E. Friberg, J. Mater. Educ., **13**, (1991) 113-131.
18. Extended Abstract, The Fifth International Conference on the Science and Technology of

Display Phosphors, San Diego, November 1999.

19. P.D. Rack, A. Naman, P.H. Holloway, S.S. Sun, R.T. Tuenge, Mat. Res. Soc. Bull. (1996) 49-58.

20. Q.H. Li, S. Komarneni, R. Roy, J. Mater. Sci. 30 (1995) 2358-2363.

21. R.N. Bhargava, D. Gallagher, and T. Welker, J. Lumin. 60&61 (1994) 275-280.

22. R.N. Bhargava, D. Gallagher, X. Hong, and A. Nurmikko, Phys. Rev. Lett. 72 (1994) 416-419.

23. A.A. Bol, and A. Meijerink, Phys. Rev. B 58 (1998) R15997-16000.

24. N. Murase, R. Jagannathan, Y. Kanematsu, M. Watanabe, A. Kurita, K. Hirata, T. Yazawa and T. Kushida, J. Phys. Chem. B 103 (1999) 754-760.

25. Y. Wang, N. Herron, K. Moller, and T. Bein, Solid State Comm. 77 (1991) 33-38.

26. T. Isobe, T. Igarashi, and M. Senna, Mat. Res. Soc. Symp. Proc. 452 (1997) 305-310.

27. C. Jin, J. Yu, L. Sun, K. Dou, S. Hou, J. Zhao, Y. Chen, and S. Huang, J. Lumin. 66&67 (1996) 315-318.

28. C. Jin, S. Hou, K. Dou, Y. Chen, S. Huang, and J. Yu, Chinese Sci. Bull. 40 (1995) 1782-1784.

29. K. Su, T.D. Tilley, M.J. Sailor, J. Am. Chem. Soc. 118 (1996) 3459-3468.

30. D. Gallagher, W.E. Heady, J.M. Racz, and R.N. Bhargava, J. Cryst. Growth 138 (1994) 970-975.

Figure Captions:

Figure 1. TEM bright field image of BT nanocrystals synthesized with a pH of 13.5 at 230 °C for 0.5 h.

Figure 2. XRD patterns of BT nanocrystals synthesized at 150 °C for 30 min from precursors with different pH values: (1) pH = 12.0, (2) pH = 12.8, (3) pH = 13.2, and (4) pH = 13.5. The vertical lines are taken from the standard cubic BT crystals JCPDS No. 31-174.

Figure 3. The DSC curve of BT nanocrystals synthesized at 230 °C for 0.5 h.

Figure 4. Structure of Tween 80 and the surface coating on nanoparticels.

Figure 5. XRD pattern of Zn_2SiO_4:Mn^{2+}phosphor particles synthesized by a seeded hydrothermal method. (1) Mn^{2+} doped Zn_2SiO_4 seeds after firing at 1000 °C for 2 h in air; (2) Mn^{2+} doped Zn_2SiO_4 phosphor particles after a hydrothermal reaction with seeds at 230 °C for 2 h; and (3) samples after a hydrothermal reaction without seeds at 230 °C for 2 h.

Figure 6. TEM image of Mn^{2+} doped Zn_2SiO_4 phosphor particles prepared by seeded hydrothermal methjod.

Figure 7. Photoluminescence spectrum (curve 1) of Mn^{2+} doped Zn_2SiO_4 phosphor particles prepared by a seeded hydrothermal method at 230 °C for 2 h. The PL spectrum (Curve 2) of Zn_2SiO_4 particles without seeds.

Figure 8. HRTEM image of Mn^{2+} doped ZnS nanoparticles.

Figure 9. XRD pattern of Mn^{2+} doped ZnS nanoparticles (mean particle size 2.6 nm calculated from peak broadening).

Figure 10. Photoluminescence enhancement by a factor of 30 from Mn^{2+} doped ZnS nanoparticles passivated by MPTS: (1) Without MPTS, (2) With MPTS, and (3) With Tween ® 80.

Figure 11. Molecular structures of MPTS, Tween80, PMMA, and polyethylene oxide.

Figure 12. Resonance and inductive effect of ester-carboxyl group.

Figure 1.

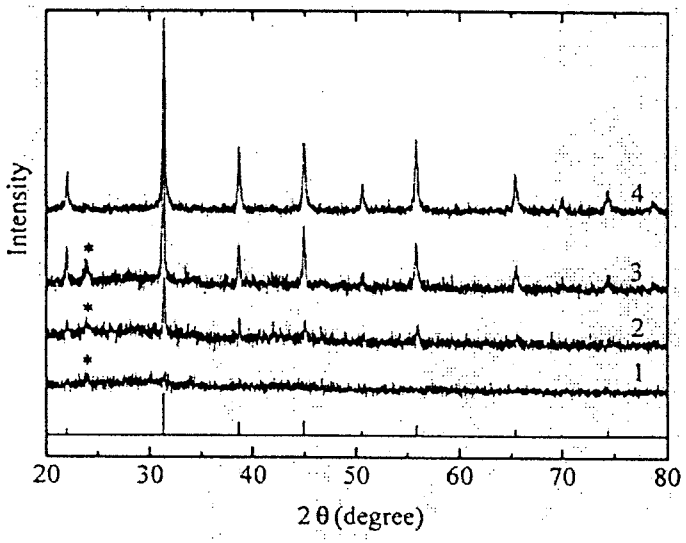

Fig. 2

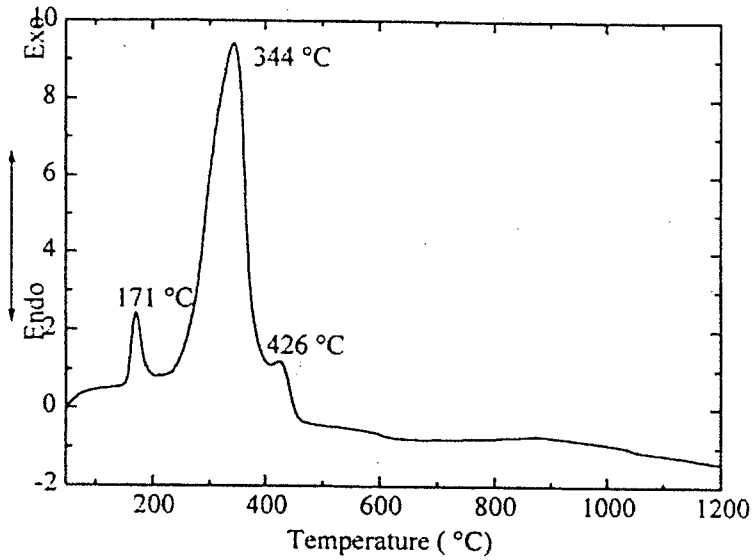
Exo
Endo
10
8
6
4
2
0
-2
344 °C
171 °C
426 °C
200
400
600
800
1000
1200
Temperature (°C)

Fig. 3

Lee & Lu

Polymer - Surface modifier and dispersant

- ▲ Tween® 80: polyoxyethylene (20) sorbitan monooleate
- ▲ Surface modifier during the hydrothermal synthesis
- ▲ Dispersant for particles in an aqueous suspension

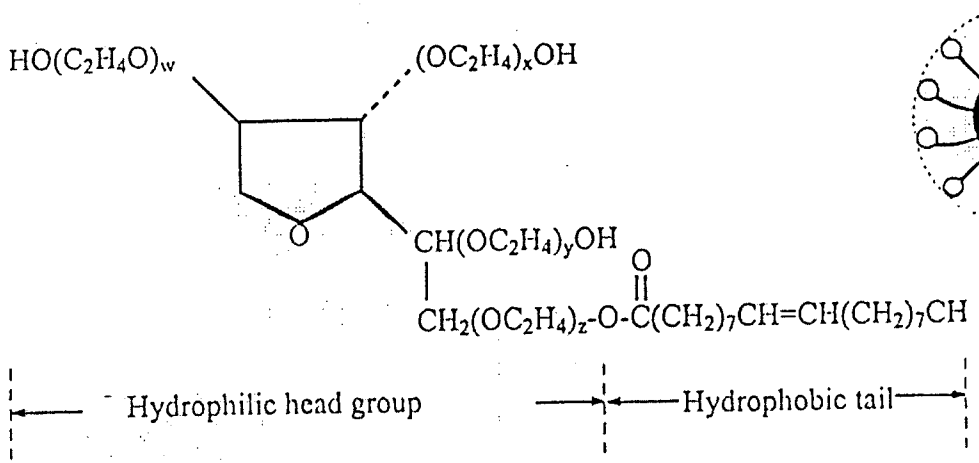

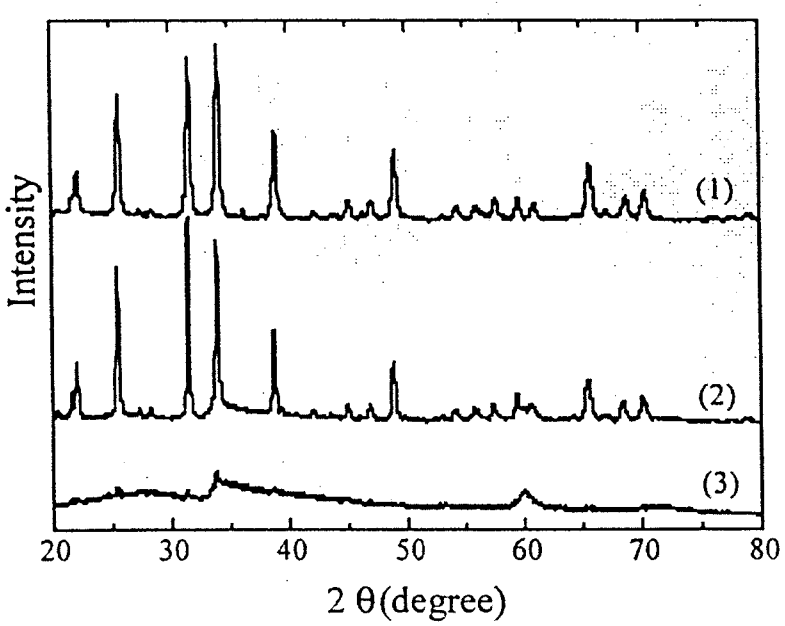

(Fig. 5)

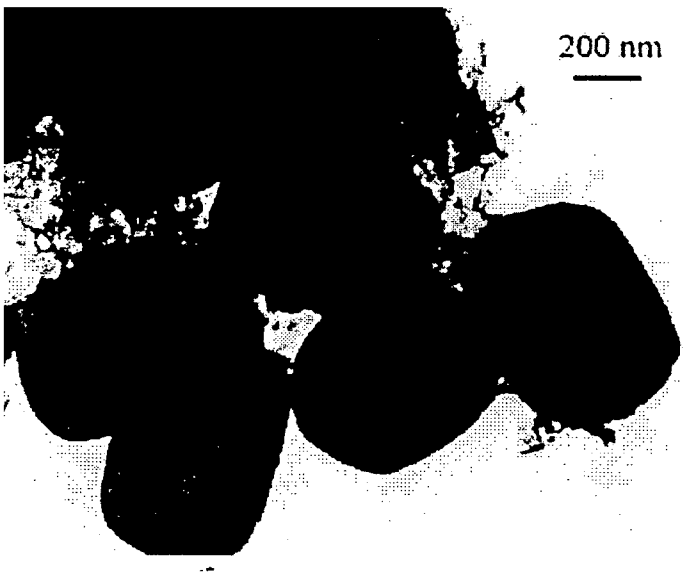

(Fig. 6)

Lee & Lu

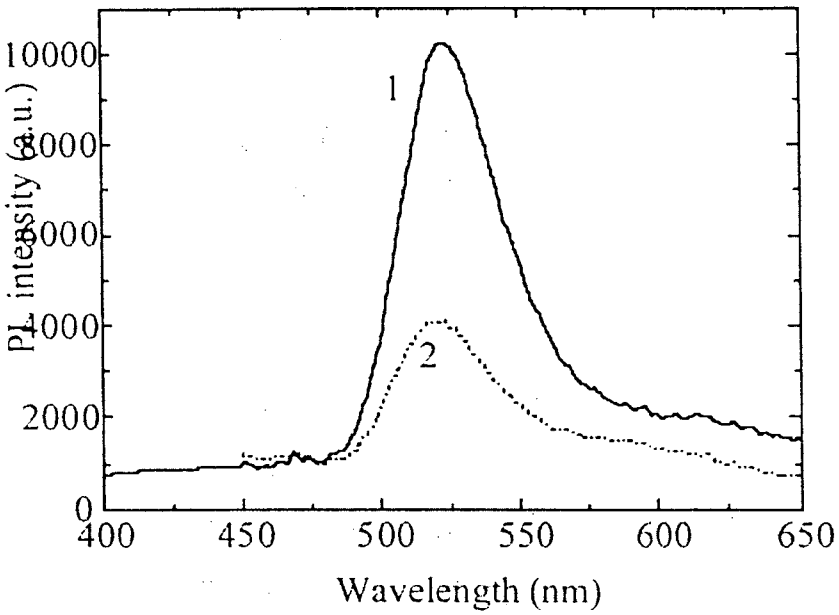
10000
8000
6000
4000
2000
0
PL intensity (a.u.)
1
2
400
450
500
550
600
650
Wavelength (nm)

Fig. 7

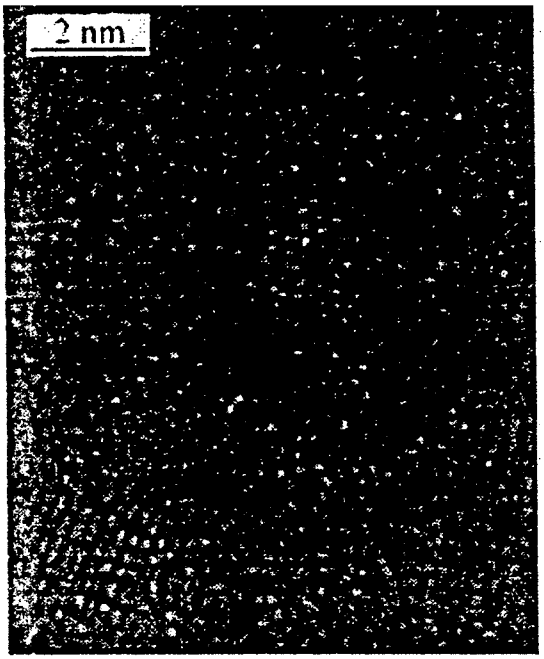

(Fig. 8)

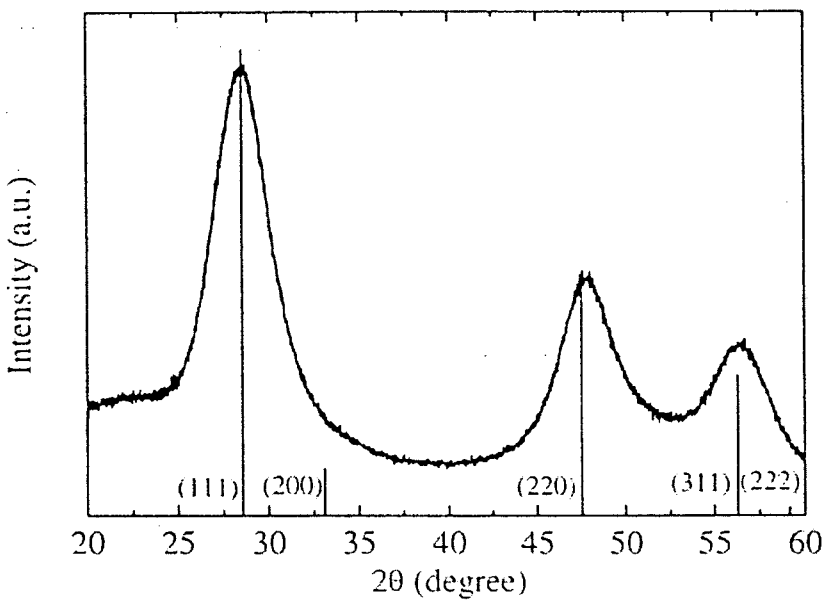
Intensity (a.u.)
(111)
(200)
(220)
(311)
(222)
20
25
30
35
40
45
50
55
60
2θ (degree)

(Figure 9)

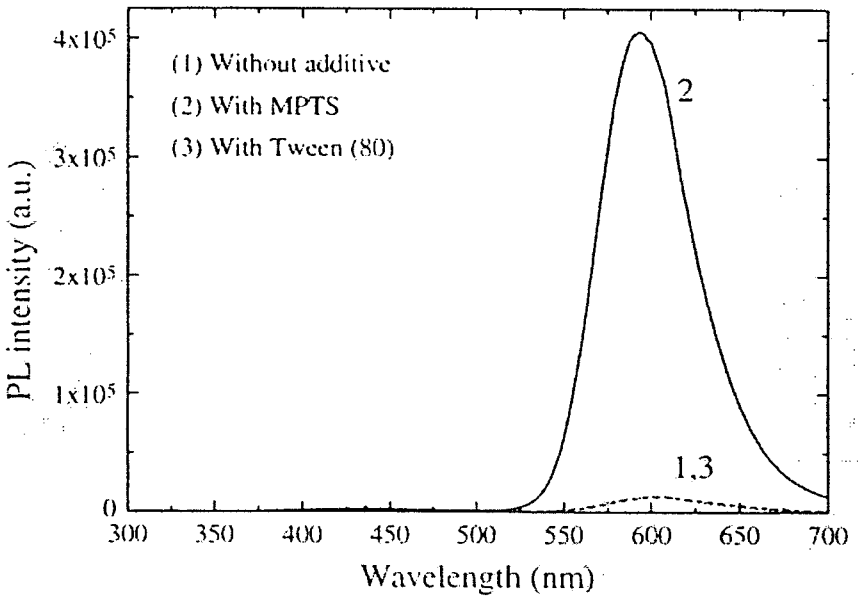
4x10⁵
3x10⁵
2x10⁵
1x10⁵
0
PL intensity (a.u.)
(1) Without additive
(2) With MPTS
(3) With Tween (80)
2
1,3
300
350
400
450
500
550
600
650
700
Wavelength (nm)

(Figure 6)

Tween 80: *polyoxyethylene (20) sorbitan monooleate*

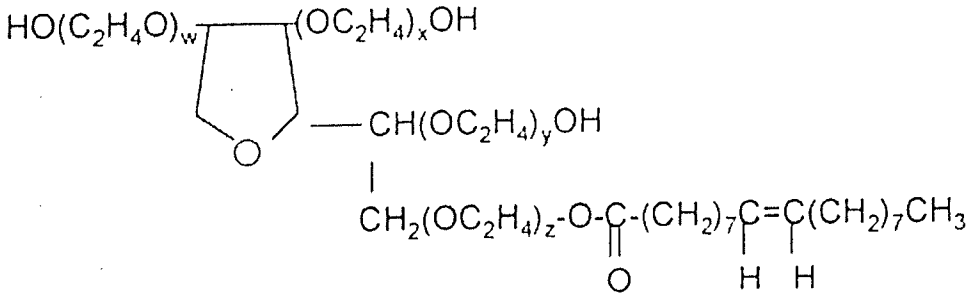

3-methacryloxypropyl trimethoxy silane (MPTS)

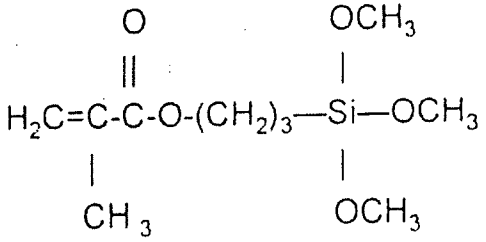

Polymethylmethacrylate (PMMA)

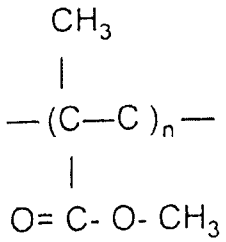

Polyethylene Oxide: $-(CH_2CH_2O)_n-$

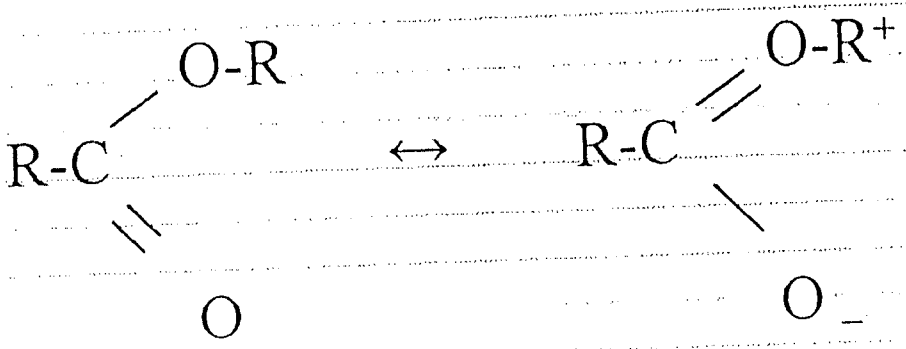

- By overlap between a 2p orbital of carbon and a 2p orbital of oxygen.
- The size of R —> Steric hindrance to adsorb on the ceramic surface.
- The inductive effect enhancing a P-type semiconduction.